

---

# Learning Chemical Reaction Representation with Reactant-Product Alignment

---

Kaipeng Zeng<sup>1</sup> Xianbin Liu<sup>1</sup> Yu Zhang<sup>1</sup> Xiaokang Yang<sup>1</sup> Yaohui Jin<sup>1</sup> Yanyan Xu<sup>1</sup>

## Abstract

Organic synthesis stands as a cornerstone of the chemical industry. The development of robust machine learning models to support tasks associated with organic reactions is of significant interest. However, current methods rely on hand-crafted features or direct adaptations of model architectures from other domains, which lack feasibility as data scales increase or ignore the rich chemical information inherent in reactions. To address these issues, this paper introduces RAlign, a novel chemical reaction representation learning model for various organic reaction-related tasks. By integrating atomic correspondence between reactants and products, our model discerns the molecular transformations that occur during the reaction, thereby enhancing comprehension of the reaction mechanism. We have designed an adapter structure to incorporate reaction conditions into the chemical reaction representation, allowing the model to handle various reaction conditions and to adapt to various datasets and downstream tasks. Additionally, we introduce a reaction-center-aware attention mechanism that enables the model to concentrate on key functional groups, thereby generating potent representations for chemical reactions. Our model has been evaluated on a range of downstream tasks. Experimental results indicate that our model markedly outperforms existing chemical reaction representation learning architectures on most of the datasets. We plan to open-source the code contingent upon the acceptance of the paper.

## 1. Introduction

Molecular design and synthesis are the core processes in the organic chemical industry, particularly in the pharmaceutical sector (Dara et al., 2022; Hasselgren & Oprea, 2024). With the surge in available data and advancements in artificial intelligence, the integration of AI into organic chemistry has achieved significant progress (Lu et al., 2018; Zhou et al., 2023). However, existing studies primarily focus on tasks related to molecular design, such as virtual screening,

which typically requires modeling of individual molecules. In contrast, tasks associated with molecular synthesis like reaction conditions prediction, which necessitate modeling the various components involved in the reaction process, are still relatively unexplored and remain a challenge for humans. These molecular synthesis-related tasks rely on effective chemical reaction representations to address the relationships among molecules during complex reaction processes. Therefore, this work focuses on the backbone design for chemical reaction representation learning, with the aim of enhancing the current state of affairs.

Existing chemical reaction representation learning methods can be roughly classified into two groups: fingerprint-based and deep learning-based. Fingerprint-based methods use hand-made fingerprints as molecular representations. These methods (Probst et al., 2022; Sandfort et al., 2020) employ various strategies to integrate the molecular representations of different components of a chemical reaction to derive a comprehensive chemical reaction representation. These representations are usually combined with conventional machine learning models, such as XGBoost (Chen & Guestrin, 2016), to tackle downstream tasks. Although these approaches do not require extensive computational resources and have proven effective with limited datasets, they may encounter performance limitations when scaling to larger datasets and more complex scenarios. This is attributed to the oversimplification of information inherent in the manually designed, statistically based features.

Working towards more powerful chemical reaction representations, researchers have increasingly turned to deep learning techniques. Using SMILES (Weininger, 1988), chemical reactions can be encoded into a string, allowing the application of natural language processing methodologies to address the challenge of chemical reaction representation learning (Lu & Zhang, 2022; Schwaller et al., 2021b). Some studies (Maser et al., 2021; Han et al., 2024) used graph neural networks for this task, taking advantage of the natural graph structure of molecules. However, most of these methods tend to directly apply existing frameworks from other domains or perform independent feature extraction for each component of the reaction followed by a simple aggregation, potentially overlooking the rich information in complex chemical reactions.

Beyond the insufficient utilization of reaction information, current methods simply regard reagents as a component of reactants for encoding when integrating reaction conditions into the reaction representation. However, this approach does not allow the model to consider any nonmolecular reaction conditions, including temperature and other environmental factors (Goodman, 2009). Furthermore, this narrow focus also impedes the applicability of current methods to datasets that provide experimental operations (e.g., stir and filter) in the form of natural language (Kearnes et al., 2021). Hence, we aim to develop a chemical reaction representation learning model that integrates a richer set of chemical information and is adaptable to various modalities of reaction conditions.

To address the aforementioned shortcomings, we proposed RAlign, a powerful chemical reaction representation learning model for multiple downstream tasks. The reaction centers and the reaction process play a pivotal role in determining the outcome of the reaction (Schwaller et al., 2021b). Drawing inspiration from the imaginary transition structures of organic reactions (Fujita, 1986), we incorporate information fusion operations for corresponding atom pairs in reactants and products within our encoder. This approach explicitly models the chemical bond changes during reactions. Furthermore, we have proposed a reaction-center-aware decoder to assist the model in focusing on key functional groups. To accommodate various modalities of reaction conditions, we have employed an adapter structure to integrate these conditions into the chemical reaction representations. We evaluated our model in a variety of tasks, including reaction condition prediction, reaction yield prediction, and reaction selectivity prediction. Our model has achieved remarkable performance across all tasks, even surpassing the baselines with extensive pretraining. **The contribution of this work can be summarized as:**

- To the best of our knowledge, this work is the first to model the atomic correspondence between reactants and products in the extraction of reaction representations and introduces the first graph-based architecture specifically tailored for chemical reactions.
- We propose a reaction condition integration mechanism that enables the model to assimilate various chemical reaction conditions and leverages previous work to enhance the chemical reaction representations.
- Extensive experiments demonstrate that our model has achieved remarkable success in a variety of tasks related to chemical reactions. In particular, our model has demonstrated a 25% increase in top-1 accuracy for reaction condition prediction task on the USPTO.CONDITION dataset, surpassing the strongest baseline.

## 2. Related Work

### 2.1. Molecular Representation Learning

Existing methods for molecule representation learning are categorized into SMILES-based and structure-based approaches. SMILES (Weininger, 1988), as a textual representation, allows molecule encoding with language models (Irwin et al., 2022), but it may overlook molecular topological information. Thus, there is a growing interest in structure-based methods, which are further divided into fingerprint-based and graph neural network (GNN)-based approaches. Fingerprint-based methods, originating from the Morgan fingerprint (Morgan, 1965), face limitations due to their manual crafting and lack of end-to-end training (Ji et al., 2023), especially with complex structures and large datasets. In contrast, GNN-based learning (Jin et al., 2017; Kao et al., 2022; Ishida et al., 2021; Yang et al., 2022; Zeng et al., 2024) has gained popularity due to its effectiveness.

Chemical reaction representation learning, crucial for industrial applications, e.g., reactivity prediction and reaction condition optimization, has seen less focus compared to molecular representation. Current chemical reaction representation learning approaches (Lu & Zhang, 2022; Schwaller et al., 2021b) often be implemented by simple concatenation of molecular representation, or rely on the straightforward application of existing backbones without domain knowledge integration. This study presents a novel model that captures molecular differences before and after reactions and incorporates reaction center information, enhancing the robustness of chemical reaction representations.

### 2.2. Reaction Condition Prediction

The chemical reaction condition prediction task aims to identify suitable catalysts, solvents, reagents, or other conditions for a given chemical reaction involving specific reactants and products. Existing methods can be broadly categorized into two types. The first category transforms the problem into a classification task within a predefined condition pool. GCNN (Maser et al., 2021) employs graph neural networks for multi-label classification to predict the presence of each molecule in the reaction condition combination. FPCR (Gao et al., 2018) and Parrot (Wang et al., 2023), focusing on reaction condition combinations with fixed compositional elements, utilize fingerprinting and BERT (Devlin et al., 2019) respectively, to predict the specific reagents for each component. The second category is not constrained by a predefined reagent library. These methods (Lu & Zhang, 2022; Andronov et al., 2023) leverage language models to generate SMILES strings of chemical reagents as reaction conditions. However, these approaches are dependent on manual feature selection based on expert knowledge and do not offer a generalizable prediction model with robust reaction representation capabilities.

### 2.3. Reaction Yield/Selectivity Prediction

Reaction yield and selectivity prediction are fundamentally similar tasks, both requiring regression of a numerical value given a chemical reaction and its conditions. Consequently, many methods are applicable to both problems. Existing strategies can be divided into two primary categories: fingerprint-based and deep learning-based. Fingerprint-based approaches construct chemical reaction representations on the basis of hand-crafted molecular fingerprints through various combinatorial strategies. DRFP (Probst et al., 2022) has designed a fingerprint that reflects the differences between reactants and products, serving as a chemical reaction representation. MFF (Sandfort et al., 2020) leverages a variety of fingerprints to enhance model performance.

Deep-learning methods predominantly employ large-scale pretrained models to extract chemical reaction representations (Schwaller et al., 2021b; Lu & Zhang, 2022; Schwaller et al., 2021c; Shi et al., 2024; Han et al., 2024), with the aim of increasing generalizability. The reaction yield prediction task often grapples with noisy data, leading some studies (Chen et al., 2024a; Kwon et al., 2022) to address this by adjusting training loss to incorporate uncertainty, thus refining model performance. In addressing reaction selectivity prediction, there is a preference for incorporating quantum chemical information. For example, the works of Li et al., Li et al. and Zahrt et al. have incorporated descriptors like average steric occupancy and electronic properties predicated on structures optimized via DFT calculations. Guan et al. designed a GNN that depends on the lowest-lying conformer calculated by DFT. However, the computation of these quantum chemical descriptors is exceedingly time-intensive, potentially necessitating several days for a modest sample size, which poses a challenge for its application to large-scale datasets. Furthermore, many deep-learning methods continue to directly apply backbone architectures from other domains. There is a clear demand for a backbone that can seamlessly integrate chemical information to extract potent chemical reaction representations, which remains an area for worthy exploration.

## 3. Preliminary

### 3.1. Notations about Chemical Reactions

In the realm of chemical reactions, the fundamental components are reactants and products. These can be represented as two distinct molecular graphs, denoted by  $G_R = (V_R, E_R)$  and  $G_P = (V_P, E_P)$  respectively. Here,  $V_P$  and  $V_R$  represent the set of atoms, while  $E_P$  and  $E_R$  represent the chemical bonds that interconnect them.

A cardinal principle in chemical reactions is the conservation of atoms. This principle dictates that for every atom present in the products, there exists a unique correspond-

ing atom in the reactants. Let  $V_R = \{v_1^R, v_2^R, \dots, v_n^R\}$  and  $V_P = \{v_1^P, v_2^P, \dots, v_m^P\}$  with  $n \geq m$ . For clarity and consistency in subsequent discussions, we stipulate that for all  $1 \leq i \leq m$ , the atom  $v_i^R$  is the unique counterpart to the atom  $v_i^P$  in the products. And we define the atoms of reactants that do not appear in the products as the leaving group, denoted as  $V_L = \{v_{m+1}^R, v_{m+2}^R, \dots, v_n^R\}$ .

We further denote the set of reaction centers as  $V_{rc}$ , which is a subset of all atoms of both reactants and products. An atom is considered as a reaction center as long as it meets one of the following criteria:

- It is an atom from either the reactants or products that is the terminus of a chemical bond undergoing alteration during the reaction.
- It is an atom from the reactants (or products) whose hydrogen count is discordant with that of its corresponding atom in the products (or reactants).
- It is an atom that is a one-hop neighbor of an atom satisfying the first two conditions.
- It is a part of the leaving group.

The above definitions are extensions derived from the common definitions of reaction centers used in retrosynthesis, which are inspired by Retroformer (Wan et al., 2022).

### 3.2. Reaction Selectivity Prediction

The same set of reactants can produce different products under varying conditions. The task of reaction selectivity prediction aims to forecast the proportions of different products that can be generated from a given set of reactants under specified conditions. Reaction selectivity usually includes regio-selectivity and chiral-selectivity. The former refers to the production of different products due to differences in reaction sites, while the latter refers to the production of a pair of mirror-symmetrical products. The tendency to produce a certain product is related to the corresponding intermediate state energy, which is termed  $\Delta G^\ddagger$ . Previous work (Seeman, 1986) on transition state theory indicates that there is an exponential relationship between  $\Delta G^\ddagger$  and the chemical reaction rate, which means that the lower the energy of the intermediate state, the higher the reaction rate and the more inclined to form the corresponding product. To be specific (Nakliang et al., 2021), the reaction ratio of producing product  $A$  and  $B$  could be formulated as:

$$\frac{r_A}{r_B} = \exp \frac{\Delta \Delta G^\ddagger}{RT} \quad (1)$$

where  $R$  is gas constant,  $T$  is the Kelvin temperature, and  $\Delta \Delta G^\ddagger$  represents the differences in  $\Delta G^\ddagger$  between different

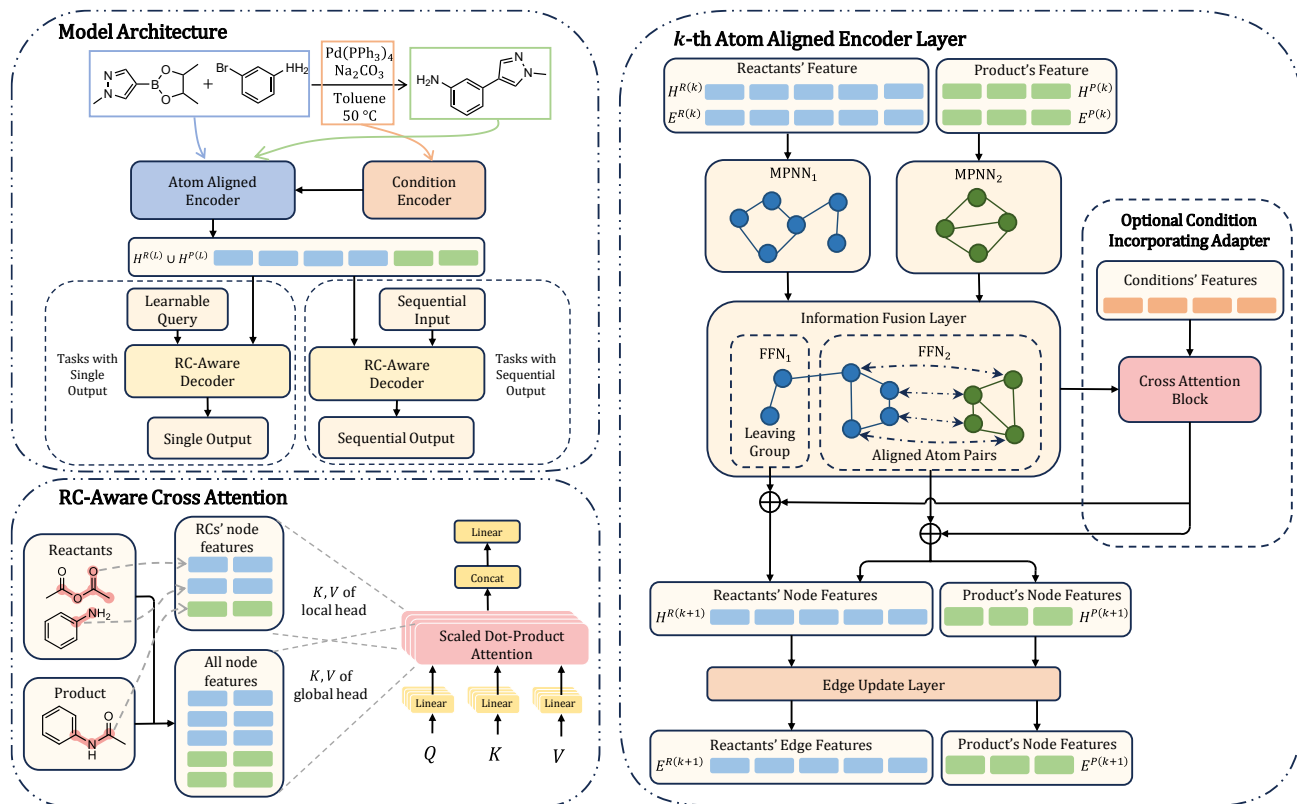


Figure 1. Overview of RAlign. For a given chemical reaction, the molecule graphs of reactants and products, along with their atomic correspondence, are input into a  $L$ -layer Atom Aligned Encoder to extract reaction node features  $H^{P(L)}$  and  $H^{R(L)}$ . If the reaction conditions are also provided, they are encoded by a condition encoder and merged into  $H^{P(L)}$  and  $H^{R(L)}$  via an adapter structure proposed in this study. The resulting features are then processed by the RC-aware decoder to produce outputs for subsequent tasks. We have tailored two decoders for both sequential output and single output, both featuring an RC-aware cross-attention layer to concentrate on key reaction motifs.

reaction pathways for product  $A$  and  $B$ . In most cases, people use the ratio of the product  $A$  and  $B$ , i.e.,  $\frac{r_A}{r_B}$ , to approximate the selectivity of chemical reactions. Then the reaction selectivity prediction, which might involve multiple reactions and products, can be simplified into the prediction of  $\Delta G^\ddagger$  of a chemical reaction with a single product.

### 3.3. Reaction Condition Combination Generation / Prediction

In this paper, the term “reaction condition combinations” specifically refers to the combination of catalysts, solvents, and other chemical reagents. The distinction between the prediction task and the generation task lies in the fact that the prediction task utilizes a predefined library of chemical reagents from which appropriate combinations are selected; on the contrary, the generation task does not require a predefined library and the model must generate suitable molecular combinations *de novo*.

## 4. Methodology

We introduce a novel chemical reaction feature extractor named RAlign with an encoder-decoder architecture, as illustrated in Fig. 1. The encoder incorporates the atomic correspondence between reactants and products to generate robust features for the chemical reaction. The decoder then integrates the output features from the encoder according to the reaction center information to produce differently formatted outputs customized to downstream tasks.

### 4.1. Atom Aligned Encoder

Understanding chemical reaction mechanisms is fundamental to developing robust representations in cheminformatics. Despite significant advancements, our grasp of these mechanisms remains incomplete, and the annotation of reaction mechanisms necessitates considerable effort from chemical experts. To navigate this challenge, we have adopted a pragmatic approach. Currently, there are well-established

tools (Schwaller et al., 2021a; Chen et al., 2024b) that can delineate the atomic correspondence between reactants and products in chemical reactions. Integrating this atomic mapping information into models can enhance the identification of similarities and differences between reactants and products, thereby improving the model’s capacity to understand the evolution of chemical reactions. Driven by these considerations, we introduce the Atom Aligned Encoder, a model engineered to assimilate both the chemical reaction and its associated atom-mapping data for effective encoding of chemical reactions.

The Atom Aligned Encoder is structured as a series of identical blocks that iteratively refine the node and edge features, mirroring the iterative process of GNNs. Within each block, we deploy two distinct message-passing neural network (MPNN) layers for reactants and products, respectively. These layers amalgamate both node and edge features in accordance with the molecular structures, yielding intermediate node features. Subsequently, an information fusion layer is implemented to integrate intermediate features of corresponding atom pairs between reactants and products. Additionally, the intermediate node features of atoms that are absent in the products are further refined through an auxiliary feedforward network. Ultimately, the edge features are updated based on the node features of the edge termini.

Given a chemical reaction with reactants  $R = (V_R, E_R)$  and products  $P = (V_P, E_P)$ , where  $V_R = \{v_1^R, v_2^R, \dots, v_n^R\}$  and  $V_P = \{v_1^P, v_2^P, \dots, v_m^P\}$ , we denote the output node feature of  $k$ -th block for  $v_i^R$  (resp.  $v_i^P$ ) as  $h_i^{R(k)}$  (resp.  $h_i^{P(k)}$ ) and the output edge feature of the  $k$ -th block for  $(v_i^R, v_j^R) \in E_R$  (resp.  $(v_i^P, v_j^P) \in E_P$ ) as  $e_{i,j}^{R(k)}$  (resp.  $e_{i,j}^{P(k)}$ ). We further delineate the collection of the output node features and edge features for both reactants and products of the  $k$ -th block, as articulated in Eq. 2.

$$\begin{aligned} H^{R(k)} &= \{h_1^{R(k)}, h_2^{R(k)}, \dots, h_n^{R(k)}\}, \\ H^{P(k)} &= \{h_1^{P(k)}, h_2^{P(k)}, \dots, h_m^{P(k)}\}, \\ E^{R(k)} &= \{e_{i,j}^{R(k)} \mid (v_i^R, v_j^R) \in E_R\}, \\ E^{P(k)} &= \{e_{i,j}^{P(k)} \mid (v_i^P, v_j^P) \in E_P\}. \end{aligned} \quad (2)$$

Then the  $k$ -th block of Atom Aligned Encoder can be math-

ematically summarized as

$$\begin{aligned} \{\tilde{h}_i^{R(k)}, \tilde{h}_i^{R(k)}, \dots, \tilde{h}_i^{R(k)}\} &= \text{MPNN}_1 \left( H^{R(k-1)}, E^{R(k-1)} \right), \\ \{\tilde{h}_i^{P(k)}, \tilde{h}_i^{P(k)}, \dots, \tilde{h}_i^{P(k)}\} &= \text{MPNN}_2 \left( H^{P(k-1)}, E^{P(k-1)} \right), \\ \left[ h_i^{R(k)} \parallel h_i^{P(k)} \right] &= \text{FFN}_1 \left( \left[ \tilde{h}_i^{R(k)} \parallel \tilde{h}_i^{P(k)} \right] \right), 1 \leq i \leq m, \\ h_i^{R(k)} &= \text{FFN}_2 \left( \tilde{h}_i^{R(k)} \right), m < i \leq n, \\ e_{i,j}^{R(k)} &= \text{FFN}_3 \left( \left[ h_i^{R(k)} \parallel h_j^{R(k)} \right] \right), \\ e_{i,j}^{P(k)} &= \text{FFN}_4 \left( \left[ h_i^{P(k)} \parallel h_j^{P(k)} \right] \right), \end{aligned} \quad (3)$$

where  $[\cdot \parallel \cdot]$  represents the concatenation of features,  $H^{R(0)}$ ,  $H^{P(0)}$ ,  $E^{R(0)}$  and  $E^{P(0)}$  represent the initial node and edge features for reactants and products. In Eq. 3,  $\tilde{h}_i^{R(k)}$  (resp.  $\tilde{h}_i^{P(k)}$ ) represents the intermediate features of the  $k$ -th block for  $v_i^R$  (resp.  $v_i^P$ ). Residual connections and layer normalization (Ba et al., 2016) are implemented across different layers to expedite model convergence and facilitate the stabilization of the training process. The detailed implementation of initial feature extraction and the message passing network is presented in Appendix C.

## 4.2. Incorporating Reaction Conditions

The formatting of chemical reaction conditions varies across different datasets, contingent upon the specific application scenarios. Moreover, the conditions of chemical reactions might incorporate multimodal information. For example, the Reaxys dataset (Wang et al., 2023) details reaction conditions by specifying supplementary reagents and precise temperatures. Conversely, in the research conducted by Yoshikawa et al. (Yoshikawa et al., 2023), these conditions are translated into a uniform series of experimental protocols. Furthermore, in predictive tasks such as forecasting reaction conditions, reaction conditions will not be provided as input. This underscores the necessity for a modular design in the chemical reaction condition incorporation module, one that can be easily interchanged or omitted, rather than being a rigid component of the encoder architecture. Consequently, we propose a versatile mechanism for integrating chemical reaction conditions, ensuring its adaptability to a range of applications within the field of cheminformatics.

Drawing inspiration from multimodal conditional image generation works such as T2IAdapter (Mou et al., 2024) or ControlNet (Zhang et al., 2023), which adeptly integrate multimodal information and effectively leverage prior research to enhance model performance, we have chosen to implement an adapter structure for incorporating reaction conditions. This approach allows us to seamlessly assimilate these conditions without necessitating modifications to the underlying architecture of the Atom Aligned Encoder. Let

us assume that the reaction condition for a given reaction has been encoded into a feature matrix  $C \in \mathbb{R}^{c \times d}$ , where  $c$  denotes the number of features and  $d$  signifies the dimension of each feature. For each block within the Atom Aligned Encoder, we utilize multi-head attention to integrate the reaction condition information into its output node features. Subsequently, we employ these node features, now imbued with reaction condition information, to generate the output edge features. Mathematically, with the incorporation of chemical reaction conditions, the output node features and edge features of the  $k$ -th block in Atom Aligned Encoder are modified as follows:

$$\begin{aligned} \left[ \dot{h}_i^{R(k)} \parallel \dot{h}_i^{P(k)} \right] &= \text{FFN}_1 \left( \left[ \tilde{h}_i^{R(k)} \parallel \tilde{h}_i^{P(k)} \right] \right), 1 \leq i \leq m, \\ \dot{h}_i^{R(k)} &= \text{FFN}_2 \left( \tilde{h}_i^{R(k)} \right), m < i \leq n, \\ \dot{h}_i^{R(k)} &= \dot{h}_i^{R(k)} + \text{Attn}_1 \left( \dot{h}_i^{R(k)}, C, C \right), \\ \dot{h}_i^{P(k)} &= \dot{h}_i^{P(k)} + \text{Attn}_2 \left( \dot{h}_i^{P(k)}, C, C \right), \\ e_{i,j}^{R(k)} &= \text{FFN}_3 \left( \left[ \dot{h}_i^{R(k)} \parallel \dot{h}_j^{R(k)} \right] \right), \\ e_{i,j}^{P(k)} &= \text{FFN}_4 \left( \left[ \dot{h}_i^{P(k)} \parallel \dot{h}_j^{P(k)} \right] \right), \end{aligned} \quad (4)$$

where the intermediate node features  $\tilde{h}_i^{R(k)}$  and  $\tilde{h}_i^{P(k)}$ , as described in Eq. 3, are the outputs of the MPNN layer.  $\text{Attn}(Q, K, V)$  in Eq. 4 denotes the vanilla multihead attention (Vaswani et al., 2017), which can be mathematically expressed as

$$\begin{aligned} o_i &= \text{softmax} \left( \frac{QW_i^Q(KW_i^K)^T}{\sqrt{d}} \right) VW_i^V, \\ \text{Attn}(Q, K, V) &= [o_1 \parallel o_2 \parallel \dots \parallel o_h] W^O \end{aligned} \quad (5)$$

where  $W_i^Q, W_i^K, W_i^V$  and  $W^O$  are learnable parameters,  $[\cdot \parallel \cdot]$  represents the concatenation of features,  $h$  is the number of heads and  $d$  is the dimension of the key vectors.

### 4.3. Reaction-Center-Aware Decoders

The decoder takes the encoded node features  $H^{R(L)}$  and  $H^{P(L)}$  from Atom-Aligned Encoder with  $L$  blocks as input and generates outputs in various formats depending on the task at hand. In this section, we introduce decoder architectures tailored for both sequential generation tasks and tasks with a single output. Given that reaction centers record key functional groups involved in chemical reactions and play a decisive role in their properties (Keto et al., 2024), we have designed a Reaction-Center-Aware Decoder that explicitly integrates information about reaction centers into chemical reaction representations applied to downstream tasks.

We first introduce the Reaction-Center-Aware (RC-aware) cross-attention mechanism, which is adapted from the local-

global decoder of the Retroformer (Wan et al., 2022). RC-aware cross-attention is a specialized attention mechanism in which half of the attention heads function identically to standard attention, while the other half is restricted to accessing only the node features of the reaction centers  $V_{rc}$ . The formulation for attention heads  $i$  within the RC-aware cross-attention mechanism, which are constrained to accessing only the reaction centers, is articulated as follows:

$$\begin{aligned} \alpha_i^1 &= \frac{\exp(k_i^R q^T)}{\sum_{v_j^R \in V_{rc}} \exp(k_j^R q^T) + \sum_{v_j^P \in V_{rc}} \exp(k_j^P q^T)}, \\ \alpha_i^2 &= \frac{\exp(k_i^P q^T)}{\sum_{v_j^R \in V_{rc}} \exp(k_j^R q^T) + \sum_{v_j^P \in V_{rc}} \exp(k_j^P q^T)}, \\ o_i &= \sum_{v_l^R \in V_{rc}} \frac{\alpha_i^1}{\sqrt{d}} h_l^{R(L)} W_i^V + \sum_{v_l^P \in V_{rc}} \frac{\alpha_i^2}{\sqrt{d}} h_l^{P(L)} W_i^V, \\ [k_i^R, k_i^P, q] &= [h_l^{R(L)} W_i^K, h_l^{P(L)} W_i^K, QW_i^Q], \end{aligned} \quad (6)$$

where  $W_i^Q, W_i^K, W_i^V$  are learnable parameters,  $Q$  is the query vector and  $d$  is the dimensionality of the key vectors. The output of RC-aware cross-attention is summarized as

$$\text{RCAttn}(Q, H^{R(L)} \cup H^{P(L)}, V_{rc}) = [o_1 \parallel o_2 \parallel \dots \parallel o_h] W^O, \quad (7)$$

where  $W^O$  is a learnable parameter,  $[\cdot \parallel \cdot]$  represents the concatenation of features and  $h$  is the number of heads.

Then for sequential generation tasks, we replace the cross-attention layers of the vanilla transformer decoder (Vaswani et al., 2017) with RC-aware cross-attention, thus customizing our decoder. In the case of tasks that require a numerical output, such as chemical reaction yield prediction, we utilize a learnable query vector within the RC-aware cross-attention mechanism to derive a reaction-level representation. Subsequently, this representation is fed into a feed-forward network to generate the final output.

## 5. Experiments

To demonstrate the capability of our model to extract potent reaction embeddings and its adaptability to various downstream tasks, we conducted extensive experiments, including predictions of reaction condition combinations, reaction yield, and reaction selectivity. For ease of understanding, we have depicted the pipelines for different tasks in Fig 9.

### 5.1. Reaction Condition Combination Prediction/Generation

**Dataset.** We use the USPTO\_CONDITION dataset to evaluate the performance of our model on the reaction condition combination prediction task. This dataset comprises 680,741 reactions, with each reaction condition consistently consisting of one catalyst, two reagents, and two solvents.

Table 1. Accuracy of each component on USPTO\_CONDITION dataset for reaction condition prediction. The detailed prediction accuracy on each type of components is displayed. The best performance is in bold and the second-best is underlined.

Method	Top- <i>k</i> accuracy (%)											
	catalyst				solvents				reagents			
	1	3	5	10	1	3	5	10	1	3	5	10
Parrot-LM-E	<u>92.12</u>	<u>94.91</u>	<u>95.97</u>	<u>97.28</u>	44.20	59.23	63.71	66.16	46.47	<u>62.04</u>	<u>68.19</u>	<u>73.93</u>
GCNN	90.59	91.80	92.40	93.39	32.39	46.02	52.51	61.06	35.84	46.37	50.61	55.99
Reagent Transformer	89.80	93.30	94.52	95.88	37.97	51.29	57.47	65.44	39.11	55.20	61.83	69.80
FPRCR	91.22	92.82	93.57	94.74	38.51	49.72	54.64	61.56	37.54	47.95	52.69	58.48
T5Chem	88.60	92.38	93.68	95.07	30.30	46.66	54.63	64.57	32.71	47.98	54.86	63.25
Ours	<b>92.98</b>	<b>95.75</b>	<b>96.60</b>	<b>97.52</b>	<b>50.45</b>	<b>66.81</b>	<b>72.75</b>	<b>79.18</b>	<b>49.68</b>	<b>63.46</b>	<b>68.69</b>	<b>75.21</b>

Table 2. Overall accuracy of reaction condition prediction on USPTO\_CONDITION dataset. The best performance is in bold. The second-best performance is underlined.

Model	Top- <i>k</i> accuracy (%)			
	1	3	5	10
GCNN	12.81	21.95	26.40	32.17
FPRCR	16.90	26.38	31.16	36.96
Reagent Transformer	22.74	34.09	39.36	46.01
Parrot-LM-E	<u>27.42</u>	<u>41.86</u>	<u>46.98</u>	<u>50.95</u>
T5Chem	16.42	27.75	33.53	40.79
Ours	<b>34.30</b>	<b>47.60</b>	<b>52.82</b>	<b>59.22</b>

Table 3. Overall accuracy of reaction condition generation on USPTO\_500MT dataset. The best performance is in bold. The second-best performance is underlined.

Model	Top- <i>k</i> accuracy (%)			
	1	3	5	10
T5Chem-pretrained	<u>25.36</u>	<u>38.12</u>	<u>43.42</u>	<u>49.54</u>
GCNN	4.74	12.36	17.94	24.58
Reagent Transformer	17.88	25.47	28.78	33.27
T5Chem-from-scratch	17.32	28.21	32.98	38.76
Ours	<b>26.91</b>	<b>39.80</b>	<b>44.82</b>	<b>50.73</b>

We have directly used the data processed by Wang et al. and further employed RXNMapper (Schwaller et al., 2021a) to augment chemical reactions with atom mapping. For the reaction condition combination generation task, we use the USPTO\_500MT dataset for evaluation. We generate and sort the reagents according to a certain rule, whose details are displayed in Appendix D.2. The tokenization on the SMILES representations of the reagents is aligned with the work (Schwaller et al., 2019). We use the top-*k* accuracy to evaluate both prediction and generation tasks; the details are illustrated in Appendix B.2.

**Baselines.** We choose T5Chem (Lu & Zhang, 2022), GCNN (Maser et al., 2021) and Reagent Transformer (Andronov et al., 2023) as our baselines on both the USPTO\_500MT and the USPTO\_CONDITION datasets. For the USPTO\_CONDITION dataset, we compared two more baselines, Parrot-LM-E (Wang et al., 2023) and FPRCR (Gao et al., 2018), which are designed for reaction condition combinations with a fixed number of components. Additionally, we reported the performance of T5Chem finetuned from the pretrained checkpoint on the USPTO\_500MT dataset. The details of the baselines are in Appendix E.

**Performance Evaluation.** The results of the USPTO\_CONDITION dataset are summarized in Table 2 and Table 1. And the results of USPTO\_500MT are summarized in Table 3. From the table, we can find that

in the USPTO\_CONDITION dataset, our model achieves a top-1 accuracy of 34.30%, a top-5 accuracy of 52.82%, and a top-10 accuracy of 59.22%, surpassing the strongest baseline Parrot-LM-E by 6.88%, 5.84%, and 8.27%, respectively. When evaluating the prediction accuracy for each type of component within reaction conditions, it is observed that our model significantly outperforms all baseline models across all metrics. Particularly in the prediction of solvents, our model attains a top-1 accuracy of 50.45% and a top-10 accuracy of 79.18%, surpassing the strongest baseline by 6.25% and 13.02%, respectively. On the USPTO\_500MT dataset, our model achieves a top-1 overall accuracy of 26.91% and a top-10 overall accuracy of 50.73%, which exceeds the strongest baseline that did not utilize pretraining by 9.03% and 11.93%. It can be observed that our model outperforms the T5Chem model pretrained on a large-scale reaction dataset. The aforementioned performance indicates that our model is capable of extracting robust reaction representations for both predictive and generative tasks.

## 5.2. Reaction Yield Prediction

**Dataset.** We use the Buchwald-Hartwig data set (Ahneman et al., 2018) to evaluate the performance of our model on the reaction yield prediction task. The dataset provides 10 random splits and four ligand-based out-of-sample splits for evaluation. The test sets under the four out-of-sample

Table 4. The results on Buchwald-Hartwig dataset under four out-of-sample split. The best performance is in **bold**. The second-best performance is underlined.

Model	Test1			Test2			Test3			Test4		
	MAE ↓	RMSE ↓	$R^2$ ↑	MAE ↓	RMSE ↓	$R^2$ ↑	MAE ↓	RMSE ↓	$R^2$ ↑	MAE ↓	RMSE ↓	$R^2$ ↑
MFF	9.7774	14.2630	0.7263	9.7732	14.2123	0.7248	9.6202	14.9177	0.7181	14.7023	19.8501	0.4367
DRFP	7.9492	11.3285	0.8273	9.0878	13.5990	0.7480	10.0901	15.8577	0.6814	<u>12.7572</u>	<u>19.1300</u>	0.4769
Chemprop	8.5883	12.3130	0.7960	10.5984	14.2913	0.7217	10.4930	15.4690	0.6969	14.5839	20.4564	0.4018
YieldBert	7.5416	<u>11.2156</u>	0.8308	7.4349	10.8098	0.8408	9.6488	15.2584	0.7051	13.5600	19.3862	0.4627
T5Chem	<u>7.1283</u>	11.2242	<u>0.8385</u>	<u>6.7693</u>	<u>10.4041</u>	<u>0.8801</u>	<u>9.0982</u>	<u>14.3431</u>	<u>0.7665</u>	13.4069	19.7521	<b>0.6051</b>
Ours	<b>5.4643</b>	<b>8.6916</b>	<b>0.8983</b>	<b>5.4182</b>	<b>8.0480</b>	<b>0.9117</b>	<b>8.6299</b>	<b>12.4570</b>	<b>0.8034</b>	<b>12.0324</b>	<b>18.0998</b>	<u>0.5317</u>

Table 5. The results on Buchwald-Hartwig dataset under ten random splits. The best performance is in **bold**. The second-best performance is underlined.

Model	MAE ↓	RMSE ↓	$R^2$ ↑
MFF	6.4411 ± 0.8157	9.6382 ± 1.0206	0.8739 ± 0.0292
DRFP	4.0995 ± 0.1191	6.2424 ± 0.2636	0.9474 ± 0.0050
Chemprop	4.6430 ± 0.1405	6.4306 ± 0.1938	0.9441 ± 0.0042
YieldBert	<u>3.5532 ± 0.1600</u>	<u>5.4480 ± 0.3240</u>	<u>0.9599 ± 0.0050</u>
T5Chem	<b>3.5059 ± 0.1562</b>	<b>5.3181 ± 0.2482</b>	<b>0.9662 ± 0.0034</b>
Ours	3.6331 ± 0.1259	5.5649 ± 0.2839	0.9581 ± 0.0049

Table 6. The results on C-H functionalization selectivity dataset under random splits. The best performance is in bold. The second-best performance is underlined.

Model	MAE ↓	RMSE ↓	$R^2$ ↑
MFF	2.2923 ± 0.0400	2.9388 ± 0.0393	0.5891 ± 0.0095
DRFP	0.9435 ± 0.0293	1.2943 ± 0.0387	0.9203 ± 0.0042
Chemprop	<u>0.3593 ± 0.0099</u>	0.5396 ± 0.0299	0.9861 ± 0.0015
RXNFP	0.3744 ± 0.0094	<u>0.5378 ± 0.0204</u>	<u>0.9862 ± 0.0010</u>
T5Chem	0.6272 ± 0.0184	0.8213 ± 0.0226	0.9822 ± 0.0011
Ours	<b>0.3267 ± 0.0159</b>	<b>0.5110 ± 0.0292</b>	<b>0.9875 ± 0.0014</b>

data splits contain reaction additives that are not included in the training sets. We use the raw data and the data split provided by Probst et al. and add the atom mapping for reactions according to the reaction template. In this study, we have standardized the yields in a range of 0 to 100. The statistical information of different splits is summarized in Appendix B.

**Baselines.** We compare our model with four powerful baselines: DRFP (Probst et al., 2022), Chemprop (Heid et al., 2024), YieldBert (Schwaller et al., 2021c) and T5Chem (Lu & Zhang, 2022) in the yield prediction task. The details of the baselines are presented in Appendix E.

**Implementation Details.** It should be noted that the number of distinct reagents in the reaction conditions of the Buchwald-Hartwig dataset is less than 50, which makes it challenging to train a reaction condition encoder from scratch. Thus, we use a lightweight pretrained molecular encoder (Hu et al., 2020b) as our reaction condition encoder. For detailed information, please refer to Appendix C.4.

Table 7. The results on thiol addition selectivity dataset under random splits. The best performance is in bold. The second-best performance is underlined.

Model	MAE ↓	RMSE ↓	$R^2$ ↑
MFF	<b>0.1421 ± 0.0093</b>	<u>0.2122 ± 0.0169</u>	<b>0.9055 ± 0.0119</b>
DRFP	<u>0.1481 ± 0.0094</u>	<b>0.2120 ± 0.0147</b>	<u>0.9056 ± 0.0117</u>
Chemprop	0.1626 ± 0.0118	0.2283 ± 0.0174	0.8907 ± 0.0130
RXNFP	0.1650 ± 0.0111	0.2313 ± 0.0197	0.8872 ± 0.0193
T5Chem	0.1662 ± 0.0108	0.2417 ± 0.0182	0.8920 ± 0.0121
Ours	0.1535 ± 0.0085	0.2202 ± 0.0118	0.8982 ± 0.0103

**Performance Evaluation.** The average results of ten random splits of the Buchwald-Hartwig dataset are summarized in Table 5 and the results of four out-of-sample splits are summarized in Table 4. Table 5 indicates that our model has achieved an average  $R^2$  of 0.958 and an average MAE of 3.633 under ten random splits, placing it in the third position among all the compared methods. However, it is important to note that our model, which has not been pretrained on large-scale reaction data, is not significantly outperformed by two deep learning models that have. The difference in  $R^2$  between our model and the strongest baseline is less than 0.01, and the gap in terms of MAE is less than 0.1. In the out-of-sample settings, our model demonstrates superior performance under various evaluation metrics. For instance, it attains an  $R^2$  score of 0.898, surpassing the strongest baseline by 0.060. Notably, our model outperforms other baselines in all metrics, excluding the  $R^2$  metric in the Test4 data split, by a significant margin. Furthermore, our model records an approximate 2.000 improvement in RMSE across all data splits.

The aforementioned experimental results demonstrate that our model can extract powerful reaction representations even without the aid of pretraining based on large-scale chemical reaction data. Additionally, the results from the out-of-sample datasets confirm the advantages of our adapter design as mentioned in Sec. 4.2, which allows our model to conveniently leverage the previous works to enhance performance, even if such works were not specifically designed for reaction encoding.



Table 8. Effects of different modules on USPTO\_500MT Dataset for reaction condition prediction task and on the random split setting of Buchwald-Hartwig dataset for reaction yield prediction task. The best performance is in bold.

Model	USPTO_500MT				Buchwald-Hartwig		
	Top- <i>k</i> Accuracy(%)				MAE ↓	RMSE ↓	$R^2$ ↑
	1	3	5	10			
Full Version	<b>26.91</b>	<b>39.80</b>	<b>44.82</b>	50.73	<b>3.6331 ± 0.1259</b>	<b>5.5649 ± 0.2839</b>	<b>0.9581 ± 0.0049</b>
- Atom Aligned Encoder	25.69	39.00	44.51	<b>50.77</b>	3.7289 ± 0.1291	5.7318 ± 0.2520	0.9556 ± 0.0044
- Reaction-Center-Aware Decoders	26.64	39.24	44.14	50.33	3.6967 ± 0.1710	5.7845 ± 0.3948	0.9547 ± 0.0066

### 5.3. Reaction Selectivity Prediction

**Datasets.** We use the C-H functionalization dataset (Li et al., 2020) to demonstrate the predictive performance of regio-selectivity and use the experimental dataset (Zahrt et al., 2019; Li et al., 2023) regarding chiral phosphoric acid-catalyzed thiol addition to N-acylimines to illustrate the predictive performance of enantio-selectivity. There are 6114 chemical reactions in the C-H functionalization dataset, and the thiol addition dataset contains 43 catalysts and combinations of  $5 \times 5$  reactants, which form 1075 reactions. These datasets were randomly divided into a training set and a test set with a 7: 3 ratio for 10 times.

**Baseline.** Considering that the reaction selectivity prediction task is fundamentally a regression problem, we have adapted three deep learning models originally designed for reaction yield prediction, Chemprop (Heid et al., 2024), T5chem (Lu & Zhang, 2022) and RXNFP (Schwaller et al., 2021b), to this task. In addition, two fingerprint-based methods, DRFP (Probst et al., 2022) and MFF (Sandfort et al., 2020), are compared. For the details of the baselines, please refer to Appendix E.

**Performance Evaluation.** The results for two datasets are summarized in Table 6 and Table 7. On the C-H functionalization dataset, our model achieves the best performance among all methods compared on all metrics, with an average MAE of 0.327, an average RMSE of 0.511, and an average  $R^2$  of 0.988. Notably, our model outperforms two baselines RXNFP and T5chem, which are pretrained on large-scale reaction datasets. The results demonstrate that our model exhibits architectural superiority and a stronger understanding of chemical reactions compared to existing methods.

On the thiol addition dataset, two fingerprint-based methods achieve the best results. Our model ranks third with an average MAE of 0.154, an average RMSE of 0.220, and an average  $R^2$  of 0.898. Deep-learning-based models do not stand out in this dataset, which is attributed to the dataset’s sparsity, consisting of only 10 different reactants and 43 different catalysts. This sparsity is insufficient to support model training. However, it is noteworthy that our model still outperforms all other deep-learning methods, including two pretrained models, even without the aid of reaction

data pretraining, showcasing the superiority of our model architecture.

Furthermore, when dealing with extremely small-scale datasets, the performance of our model can be further enhanced by incorporating more rule-based features, such as the electronic distribution of atoms, since our model does not impose restrictions on the implementation of the MPNN network used to encode reactants and products. Large-scale pretraining on a reaction dataset will also be beneficial. However, these improvement methods are beyond the scope of this paper and will be reserved for future work.

### 5.4. Ablation Study

We investigate the effects of different components in our proposed pipelines. We remove or substitute the distinct components of our model and subject them to testing on the USPTO\_500MT dataset and the random split setting of the Buchwald-Hartwig dataset. The results are summarized in Table 8.

**Atom Aligned Encoder.** We remove the information fusion layers of the Atom Aligned Encoder. Under this circumstance, the Atom Aligned Encoder has been simplified into a network composed of two separate MPNN networks that encode reactants and products, respectively. As observed in Table 8, the removal of the information fusion layer has led to a decrease in model performance in both tasks, especially in terms of the top-1 and top-3 accuracy for reaction condition prediction on the USPTO\_500MT dataset. This suggests that by incorporating the alignment of atoms before and after the reaction into the model, the Atom Aligned Encoder can more effectively discern the differences between the molecules before and after the reaction, thus offering more robust reaction representations for downstream tasks.

**Reaction-Center-Aware Decoders.** We replace the RC-aware cross-attention layers with the original cross-attention layer proposed in (Vaswani et al., 2017). Table 8 demonstrates a decline in model performance in terms of all metrics for both sequential generation tasks and tasks that require a reaction-level representation. This clearly demonstrates that the RC-aware cross-attention mechanism enables the model to focus on the core functional groups of the reaction

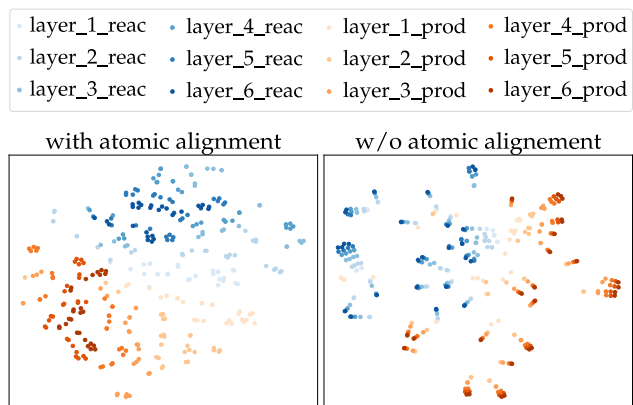


Figure 2. Different visualizations of node embeddings at each encoder layer, comparing the aligned encoder with the non-aligned encoder.

and to comprehend the reaction process, thereby leading to performance improvements.

### 5.5. Case Study

To intuitively demonstrate what our proposed module has learned, we conducted visualizations of both the embeddings learned by the atom-aligned encoder and the attention coefficients from the RC-aware cross-attention mechanism.

**The Atom-Aligned encoder helps the model learn beyond the topological structures of molecules.** To explore the changes brought about by atomic alignment for the encoder, we visualized the node embeddings generated by the atom-aligned embedding and conventional MPNN networks. The models for feature extraction were trained on the reaction condition generation task for the ablation study discussed in Sec. 5.4, and the visualizations are displayed in Fig. 2. From the figure, we can observe that due to MPNN networks only receiving topological structure information from individual molecules and the high similarity in topology between reactants and products, the node embeddings of the MPNN network are updated along almost the same pattern trajectory. Especially in the 3rd to 6th layers of the network, the spatial structure formed by the nodes does not undergo significant changes. In contrast, the atom-aligned encoder facilitates the exchange of information between different components in chemical reactions, leading to a more diverse feature space and thereby enhancing the model’s representational capacity.

**RC-aware Cross-attention helps the model to find key functional groups.** We visualize the average attention weights of different kinds of heads for predicting the catalyst of the given reaction in Fig. 3. The presented case involves the reduction of aromatic nitro groups to amino

groups using catalytic hydrogenation, a method commonly used in industry and relatively eco-friendly and efficient (Orlandi et al., 2016). However, this method is not suitable for situations where the benzene ring has other competitive groups, such as halogens (Shi, 2007; Yao & Zhang, 1984). The visualization reveals that while our RC-aware heads are restricted to focus on the reaction center, thereby providing the model with information about the reaction type, our normal heads attend to other groups on the benzene ring. This distribution of attention weights allows the model to correctly confirm the absence of other competitive groups on the benzene ring, thereby accurately predicting that the reaction can proceed via catalytic hydrogenation and precisely predicting the corresponding catalyst. The aforementioned case demonstrates that RC-aware cross-attention enables different attention mechanisms to assign clear roles to different attention heads, thereby helping the model detect and focus on key functional groups beyond the reaction center. We also provide the visualization of attention heads for predicting other components of the reaction condition and visualization for other cases in Appendix A.1.

## 6. Conclusion

In this paper, we propose RAlign, a novel chemical reaction representation learning model. Our model integrates the atomic correspondence between reactants and products, as well as information about the reaction center, enabling the model to better model the chemical bond changes and gain a deeper understanding of the reaction mechanism. An adapter is utilized to incorporate reaction conditions, allowing our model to adapt to various modalities of reaction conditions and to efficiently leverage previous work to enhance performance. Experimental results demonstrate that our model architecture outperforms existing reaction representation learning architectures across various downstream tasks. In the future, we plan to use this architecture for large-scale pretraining to use the reaction representation space to assist scientists in conducting research on reaction mechanisms.

**Limitations.** The model requires atom mappings as input. Although there are now tools for accurate atom mapping, incorrect atom mapping can still have a negative impact on the model’s performance. Like most deep learning methods, our model requires a substantial amount of training data for support; hence, on small-scale datasets, our model cannot surpass handcrafted features.

## Impact Statement

This paper introduces a novel chemical reaction representation learning architecture, designed to enhance the performance of tasks that utilize chemical reactions as input,

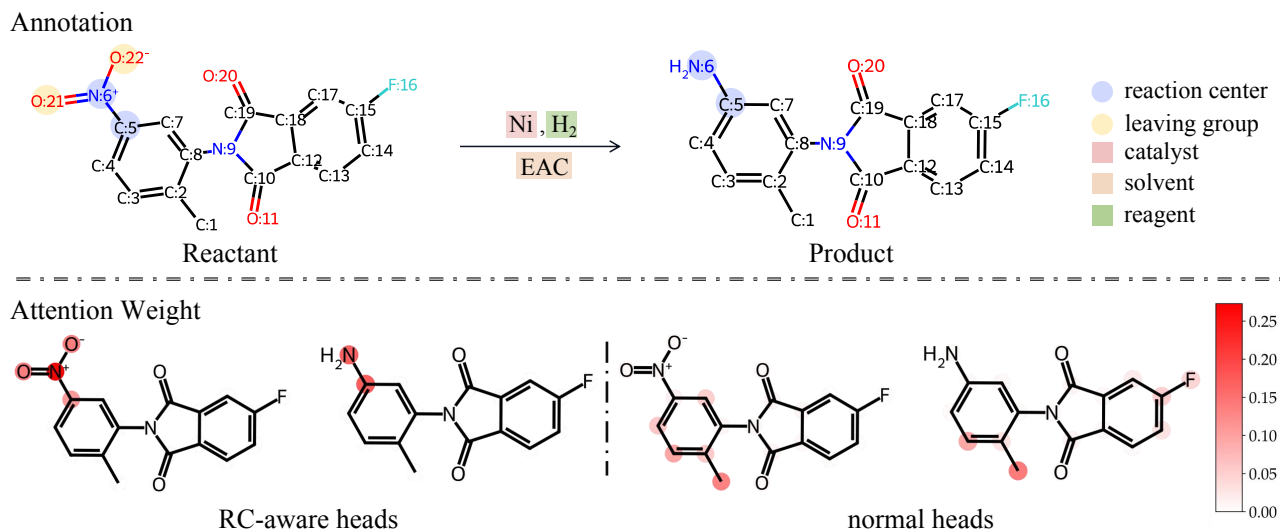


Figure 3. Visualization of RC-aware cross attention weights of each node in reactants and products for catalyst prediction

such as chemical reaction condition prediction. These tasks are intrinsically linked to the design of molecular synthesis schemes and the optimization of production processes in the organic chemical industry. Our work has the potential to increase the production efficiency of the organic synthesis industry and enable the training of more powerful reward models that align with specific demands of industrial production, thereby feeding back into upstream molecular design and related fields. It is important to note that, at present, our research does not directly engage with broader societal issues, and to date, no adverse social implications have been associated with our work.

## References

- Ahnehan, D. T., Estrada, J. G., Lin, S., Dreher, S. D., and Doyle, A. G. Predicting reaction performance in c–n cross-coupling using machine learning. *Science*, 360 (6385):186–190, 2018.
- Andronov, M., Voinarovska, V., Andronova, N., Wand, M., Clevert, D.-A., and Schmidhuber, J. Reagent prediction with a molecular transformer improves reaction data quality. *Chemical Science*, 14(12):3235–3246, 2023.
- Ba, J. L., Kiros, J. R., and Hinton, G. E. Layer normalization. *arXiv preprint arXiv:1607.06450*, 2016.
- Chen, J., Guo, K., Liu, Z., Isayev, O., and Zhang, X. Uncertainty-aware yield prediction with multimodal molecular features. In *Proceedings of the AAAI Conference on Artificial Intelligence*, volume 38, pp. 8274–8282, 2024a.
- Chen, S., An, S., Babazade, R., and Jung, Y. Precise atom-to-atom mapping for organic reactions via human-in-the-loop machine learning. *Nature Communications*, 15(1): 2250, 2024b.
- Chen, T. and Guestrin, C. Xgboost: A scalable tree boosting system. In *Proceedings of the 22nd acm sigkdd international conference on knowledge discovery and data mining*, pp. 785–794, 2016.
- Dara, S., Dhamecherla, S., Jadav, S. S., Babu, C. M., and Ahsan, M. J. Machine learning in drug discovery: a review. *Artificial intelligence review*, 55(3):1947–1999, 2022.
- Devlin, J., Chang, M., Lee, K., and Toutanova, K. BERT: pre-training of deep bidirectional transformers for language understanding. In Burstein, J., Doran, C., and Solorio, T. (eds.), *Proceedings of the 2019 Conference of the North American Chapter of the Association for Computational Linguistics: Human Language Technologies, NAACL-HLT 2019, Minneapolis, MN, USA, June 2-7, 2019, Volume 1 (Long and Short Papers)*, pp. 4171–4186. Association for Computational Linguistics, 2019. doi: 10.18653/V1/N19-1423. URL <https://doi.org/10.18653/v1/n19-1423>.
- Fey, M. and Lenssen, J. E. Fast graph representation learning with PyTorch Geometric. In *ICLR Workshop on Representation Learning on Graphs and Manifolds*, 2019.
- Fujita, S. Description of organic reactions based on imaginary transition structures. 1. introduction of new concepts. *Journal of Chemical Information and Computer Sciences*, 26(4):205–212, 1986.
- Gao, H., Struble, T. J., Coley, C. W., Wang, Y., Green, W. H., and Jensen, K. F. Using machine learning to

- predict suitable conditions for organic reactions. *ACS Central Science*, 4:1465–1476, 11 2018. ISSN 23747951. doi: 10.1021/acscentsci.8b00357.
- Goodman, J. Computer software review: Reaxys, 2009.
- Guan, Y., Coley, C. W., Wu, H., Ranasinghe, D., Heid, E., Struble, T. J., Pattanaik, L., Green, W. H., and Jensen, K. F. Regio-selectivity prediction with a machine-learned reaction representation and on-the-fly quantum mechanical descriptors. *Chemical science*, 12(6):2198–2208, 2021.
- Han, J., Kwon, Y., Choi, Y.-S., and Kang, S. Improving chemical reaction yield prediction using pre-trained graph neural networks. *Journal of Cheminformatics*, 16(1):25, 2024.
- Hasselgren, C. and Oprea, T. I. Artificial intelligence for drug discovery: Are we there yet? *Annual Review of Pharmacology and Toxicology*, 64(1):527–550, 2024.
- Heid, E., Greenman, K. P., Chung, Y., Li, S.-C., Graff, D. E., Vermeire, F. H., Wu, H., Green, W. H., and McGill, C. J. Chemprop: A machine learning package for chemical property prediction. *Journal of Chemical Information and Modeling*, 64(1):9–17, 2024. doi: 10.1021/acs.jcim.3c01250. URL <https://doi.org/10.1021/acs.jcim.3c01250>. PMID: 38147829.
- Hu, W., Fey, M., Zitnik, M., Dong, Y., Ren, H., Liu, B., Catasta, M., and Leskovec, J. Open graph benchmark: Datasets for machine learning on graphs. *Advances in neural information processing systems*, 33:22118–22133, 2020a.
- Hu, W., Liu, B., Gomes, J., Zitnik, M., Liang, P., Pande, V., and Leskovec, J. Strategies for pre-training graph neural networks. In *International Conference on Learning Representations*, 2020b. URL <https://openreview.net/forum?id=HJlWWJSFDH>.
- Irwin, R., Dimitriadis, S., He, J., and Bjerrum, E. J. Chemformer: a pre-trained transformer for computational chemistry. *Machine Learning: Science and Technology*, 3(1):015022, 2022.
- Ishida, S., Miyazaki, T., Sugaya, Y., and Omachi, S. Graph neural networks with multiple feature extraction paths for chemical property estimation. *Molecules*, 26(11):3125, 2021.
- Ji, Y., Zhang, L., Wu, J., Wu, B., Li, L., Huang, L.-K., Xu, T., Rong, Y., Ren, J., Xue, D., et al. Drugood: Out-of-distribution dataset curator and benchmark for ai-aided drug discovery—a focus on affinity prediction problems with noise annotations. In *Proceedings of the AAAI Conference on Artificial Intelligence*, volume 37, pp. 8023–8031, 2023.
- Jin, W., Coley, C., Barzilay, R., and Jaakkola, T. Predicting organic reaction outcomes with weisfeiler-lehman network. *Advances in neural information processing systems*, 30, 2017.
- Kao, Y.-T., Wang, S.-F., Wu, M.-H., Her, S.-H., Yang, Y.-H., Lee, C.-H., Lee, H.-F., Lee, A.-R., Chang, L.-C., and Pao, L.-H. A substructure-based screening approach to uncover n-nitrosamines in drug substances. *Journal of Food & Drug Analysis*, 30(1), 2022.
- Kearnes, S. M., Maser, M. R., Wlekliński, M., Kast, A., Doyle, A. G., Dreher, S. D., Hawkins, J. M., Jensen, K. F., and Coley, C. W. The open reaction database. *Journal of the American Chemical Society*, 143(45):18820–18826, 2021.
- Keto, A., Guo, T., Underdue, M., Stuyver, T., Coley, C. W., Zhang, X., Krenske, E. H., and Wiest, O. Data-efficient, chemistry-aware machine learning predictions of diels–alder reaction outcomes. *Journal of the American Chemical Society*, 6 2024. ISSN 0002-7863. doi: 10.1021/jacs.4c03131. URL <https://pubs.acs.org/doi/10.1021/jacs.4c03131>.
- Kim, S., Chen, J., Cheng, T., Gindulyte, A., He, J., He, S., Li, Q., Shoemaker, B. A., Thiessen, P. A., Yu, B., Zaslavsky, L., Zhang, J., and Bolton, E. E. PubChem in 2021: new data content and improved web interfaces. *Nucleic Acids Research*, 49(D1):D1388–D1395, 11 2020. ISSN 0305-1048. doi: 10.1093/nar/gkaa971. URL <https://doi.org/10.1093/nar/gkaa971>.
- Kingma, D. P. and Ba, J. Adam: A method for stochastic optimization. *arXiv preprint arXiv:1412.6980*, 2014.
- Kwon, Y., Lee, D., Choi, Y.-S., and Kang, S. Uncertainty-aware prediction of chemical reaction yields with graph neural networks. *Journal of Cheminformatics*, 14:1–10, 2022.
- Landrum, G. et al. Rdkit: A software suite for cheminformatics, computational chemistry, and predictive modeling. *Greg Landrum*, 8:31, 2013.
- Li, S.-W., Xu, L.-C., Zhang, C., Zhang, S.-Q., and Hong, X. Reaction performance prediction with an extrapolative and interpretable graph model based on chemical knowledge. *Nature Communications*, 14(1):3569, 2023.
- Li, X., Zhang, S.-Q., Xu, L.-C., and Hong, X. Predicting regioselectivity in radical c-h functionalization of heterocycles through machine learning. *Angewandte Chemie International Edition*, 59(32):13253–13259, 2020.
- Lu, J. and Zhang, Y. Unified deep learning model for multitask reaction predictions with explanation. *Journal of chemical information and modeling*, 62(6):1376–1387, 2022.

- Lu, X., Yang, H., Chen, Y., Li, Q., He, S.-y., Jiang, X., Feng, F., Qu, W., and Sun, H. The development of pharmacophore modeling: Generation and recent applications in drug discovery. *Current pharmaceutical design*, 24(29): 3424–3439, 2018.
- Maser, M. R., Cui, A. Y., Ryou, S., DeLano, T. J., Yue, Y., and Reisman, S. E. Multilabel classification models for the prediction of cross-coupling reaction conditions. *Journal of Chemical Information and Modeling*, 61(1): 156–166, 2021.
- Mayfield, J., Lowe, D., and Sayle, R. Pistachio: Search and faceting of large reaction databases. In *ABSTRACTS OF PAPERS OF THE AMERICAN CHEMICAL SOCIETY*, volume 254. AMER CHEMICAL SOC 1155 16TH ST, NW, WASHINGTON, DC 20036 USA, 2017.
- Morgan, H. L. The generation of a unique machine description for chemical structures—a technique developed at chemical abstracts service. *Journal of chemical documentation*, 5(2):107–113, 1965.
- Mou, C., Wang, X., Xie, L., Wu, Y., Zhang, J., Qi, Z., and Shan, Y. T2i-adapter: Learning adapters to dig out more controllable ability for text-to-image diffusion models. In *Proceedings of the AAAI Conference on Artificial Intelligence*, volume 38, pp. 4296–4304, 2024.
- Nakliang, P., Yoon, S., and Choi, S. Emerging computational approaches for the study of regio- and stereoselectivity in organic synthesis. *Organic Chemistry Frontiers*, 8(18):5165–5181, 2021.
- Orlandi, M., Brenna, D., Harms, R., Jost, S., and Benaglia, M. Recent developments in the reduction of aromatic and aliphatic nitro compounds to amines. *Organic Process Research & Development*, pp. acs.oprd.6b00205, 2016.
- Paszke, A., Gross, S., Massa, F., Lerer, A., Bradbury, J., Chanan, G., Killeen, T., Lin, Z., Gimelshein, N., Antiga, L., et al. Pytorch: An imperative style, high-performance deep learning library. *Advances in neural information processing systems*, 32, 2019.
- Probst, D., Schwaller, P., and Reymond, J.-L. Reaction classification and yield prediction using the differential reaction fingerprint drfp. *Digital Discovery*, 2022.
- Sacha, M., Błaz, M., Byrski, P., Dabrowski-Tumanski, P., Chrominski, M., Loska, R., Włodarczyk-Pruszyński, P., and Jastrzebski, S. Molecule edit graph attention network: modeling chemical reactions as sequences of graph edits. *Journal of Chemical Information and Modeling*, 61(7): 3273–3284, 2021.
- Sandfort, F., Strieth-Kalthoff, F., Kühnemund, M., Beecks, C., and Glorius, F. A structure-based platform for predicting chemical reactivity. *Chem*, 6(6):1379–1390, 2020. ISSN 2451-9294. doi: <https://doi.org/10.1016/j.chempr.2020.02.017>. URL <https://www.sciencedirect.com/science/article/pii/S2451929420300851>.
- Schwaller, P., Laino, T., Gaudin, T., Bolgar, P., Hunter, C. A., Bekas, C., and Lee, A. A. Molecular transformer: a model for uncertainty-calibrated chemical reaction prediction. *ACS central science*, 5(9):1572–1583, 2019.
- Schwaller, P., Hoover, B., Reymond, J.-L., Strobelt, H., and Laino, T. Extraction of organic chemistry grammar from unsupervised learning of chemical reactions. *Science Advances*, 7(15):eabe4166, 2021a.
- Schwaller, P., Probst, D., Vaucher, A. C., Nair, V. H., Kreutter, D., Laino, T., and Reymond, J.-L. Mapping the space of chemical reactions using attention-based neural networks. *Nature Machine Intelligence*, 3(2):144–152, 2021b.
- Schwaller, P., Vaucher, A. C., Laino, T., and Reymond, J.-L. Prediction of chemical reaction yields using deep learning. *Machine learning: science and technology*, 2(1):015016, 2021c.
- Seeman, J. I. The curtin-hammett principle and the winstein-holness equation: new definition and recent extensions to classical concepts. *Journal of Chemical Education*, 63(1):42, 1986.
- Shi, Q. *Catalytic Transfer Hydrogenation of Nitronarenes under Mild Conditions*. PhD thesis, Dalian University of Technology, 2007.
- Shi, R., Yu, G., Huo, X., and Yang, Y. Prediction of chemical reaction yields with large-scale multi-view pre-training. *Journal of Cheminformatics*, 16(1):22, 2024.
- Vaswani, A., Shazeer, N., Parmar, N., Uszkoreit, J., Jones, L., Gomez, A. N., Kaiser, Ł., and Polosukhin, I. Attention is all you need. *Advances in neural information processing systems*, 30, 2017.
- Veličković, P., Cucurull, G., Casanova, A., Romero, A., Liò, P., and Bengio, Y. Graph attention networks. In *International Conference on Learning Representations*, 2018.
- Wan, Y., Hsieh, C.-Y., Liao, B., and Zhang, S. Retroformer: Pushing the limits of end-to-end retrosynthesis transformer. In Chaudhuri, K., Jegelka, S., Song, L., Szepesvari, C., Niu, G., and Sabato, S. (eds.), *Proceedings of the 39th International Conference on Machine Learning*, volume 162 of *Proceedings of Machine Learning*, 2021.

- Learning Research*, pp. 22475–22490. PMLR, 17–23 Jul 2022. URL <https://proceedings.mlr.press/v162/wan22a.html>.
- Wang, X., Hsieh, C.-Y., Yin, X., Wang, J., Li, Y., Deng, Y., Jiang, D., Wu, Z., Du, H., Chen, H., Li, Y., Liu, H., Wang, Y., Luo, P., Hou, T., and Yao, X. Generic interpretable reaction condition predictions with open reaction condition datasets and unsupervised learning of reaction center. *Research*, 6, 1 2023. ISSN 26395274. doi: 10.34133/research.0231.
- Weininger, D. Smiles, a chemical language and information system. 1. introduction to methodology and encoding rules. *Journal of chemical information and computer sciences*, 28(1):31–36, 1988.
- Yan, C., Ding, Q., Zhao, P., Zheng, S., Yang, J., Yu, Y., and Huang, J. Retroxpert: Decompose retrosynthesis prediction like a chemist. *Advances in Neural Information Processing Systems*, 33:11248–11258, 2020.
- Yang, N., Zeng, K., Wu, Q., Jia, X., and Yan, J. Learning substructure invariance for out-of-distribution molecular representations. *Advances in Neural Information Processing Systems*, 35:12964–12978, 2022.
- Yao, M. and Zhang, R. The rogress of the reduction reaction of aromatic nitro compounds. *Chemical Industry and Engineering Progress*, (04):19–25, 1984. ISSN 1000-6613.
- Yoshikawa, N., Skreta, M., Darvish, K., Arellano-Rubach, S., Ji, Z., Bjørn Kristensen, L., Li, A. Z., Zhao, Y., Xu, H., Kuramshin, A., et al. Large language models for chemistry robotics. *Autonomous Robots*, 47(8):1057–1086, 2023.
- Zahrt, A. F., Henle, J. J., Rose, B. T., Wang, Y., Darrow, W. T., and Denmark, S. E. Prediction of higher-selectivity catalysts by computer-driven workflow and machine learning. *Science*, 363(6424):eaau5631, 2019.
- Zeng, K., Yang, B., Zhao, X., Zhang, Y., Nie, F., Yang, X., Jin, Y., and Xu, Y. Ualign: pushing the limit of template-free retrosynthesis prediction with unsupervised smiles alignment. *Journal of Cheminformatics*, 16(1):80, 2024.
- Zhang, L., Rao, A., and Agrawala, M. Adding conditional control to text-to-image diffusion models. In *Proceedings of the IEEE/CVF International Conference on Computer Vision*, pp. 3836–3847, 2023.
- Zhou, G., Gao, Z., Ding, Q., Zheng, H., Xu, H., Wei, Z., Zhang, L., and Ke, G. Uni-mol: A universal 3d molecular representation learning framework. In *The Eleventh International Conference on Learning Representations*, 2023. URL <https://openreview.net/forum?id=6K2RM6wVqKu>.

## A. Supplementary Experimental Results

### A.1. Visualization of RC-aware Cross-attention

We have supplemented the cross-attention coefficients for predicting the solvent and reagent for the case presented in Sec. 5.5, as depicted in Fig. 4. The identification of the catalyst and the provision of the reaction center have made the model aware that this reaction can be achieved through catalytic hydrogenation. Consequently, when predicting the solvent, the model’s normal attention heads focus on areas other than the benzene ring, ensuring that the proposed solvent improves reaction selectivity (i.e., the reaction proceeds at the correct site) and provides an appropriate system for its progress. This can also be observed in the normal head’s prediction of the reagent. Additionally, it is noticeable that when predicting the reagent, the model’s RC-aware heads allocate more attention to the reactant, thereby accurately predicting the reagent, hydrogen, which directly reacts with the reactant. We also provide another two cases in Fig. 5 and Fig. 6.

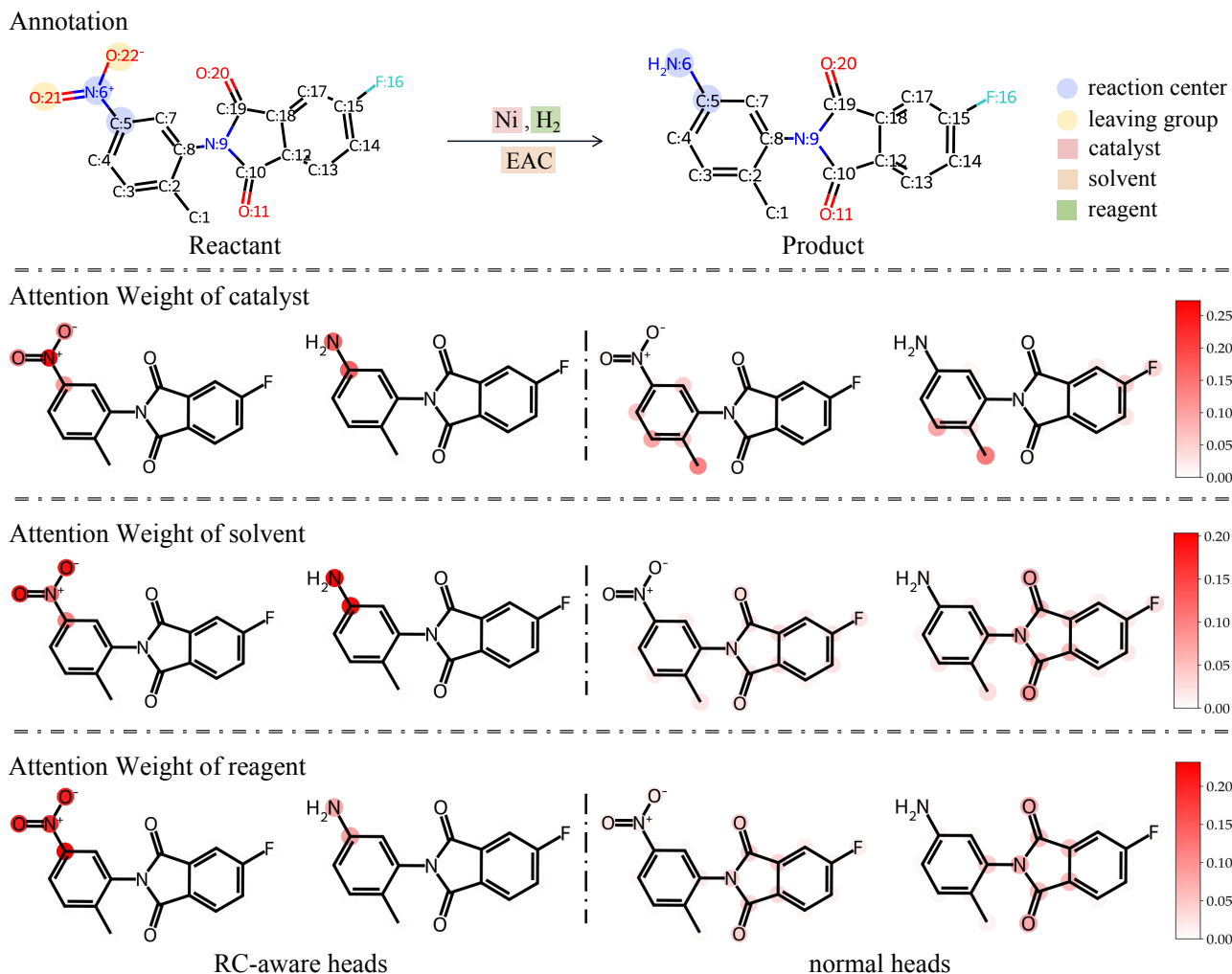


Figure 4. The visualization the attention weights of each node in reactants and products while predicting the reaction condition combination for the reduction of nitro groups.

### A.2. Embedding Visualization of Atom Aligned Encoder

We have completed the reaction information for the node embeddings shown in Sec. 5.5 and additionally provided visualizations for two more cases, which are presented in Fig. 7. We can observe that in these cases, the point features of the conventional MPNN network still follow the same patterned trajectory for updates. In contrast, our feature space appears

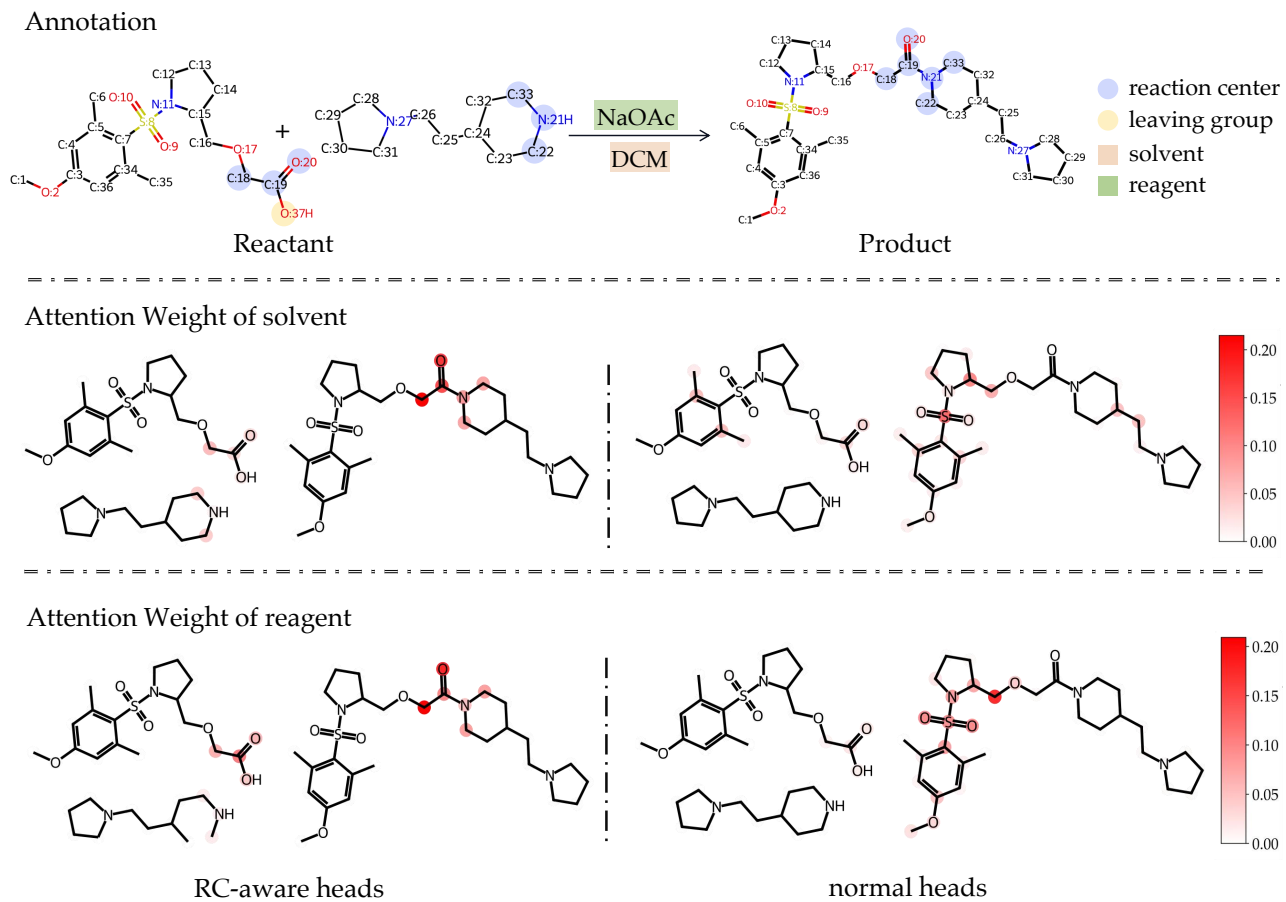


Figure 5. The visualization of the RC-aware cross attention coefficients for the reaction condition combination prediction of an amide coupling reaction.



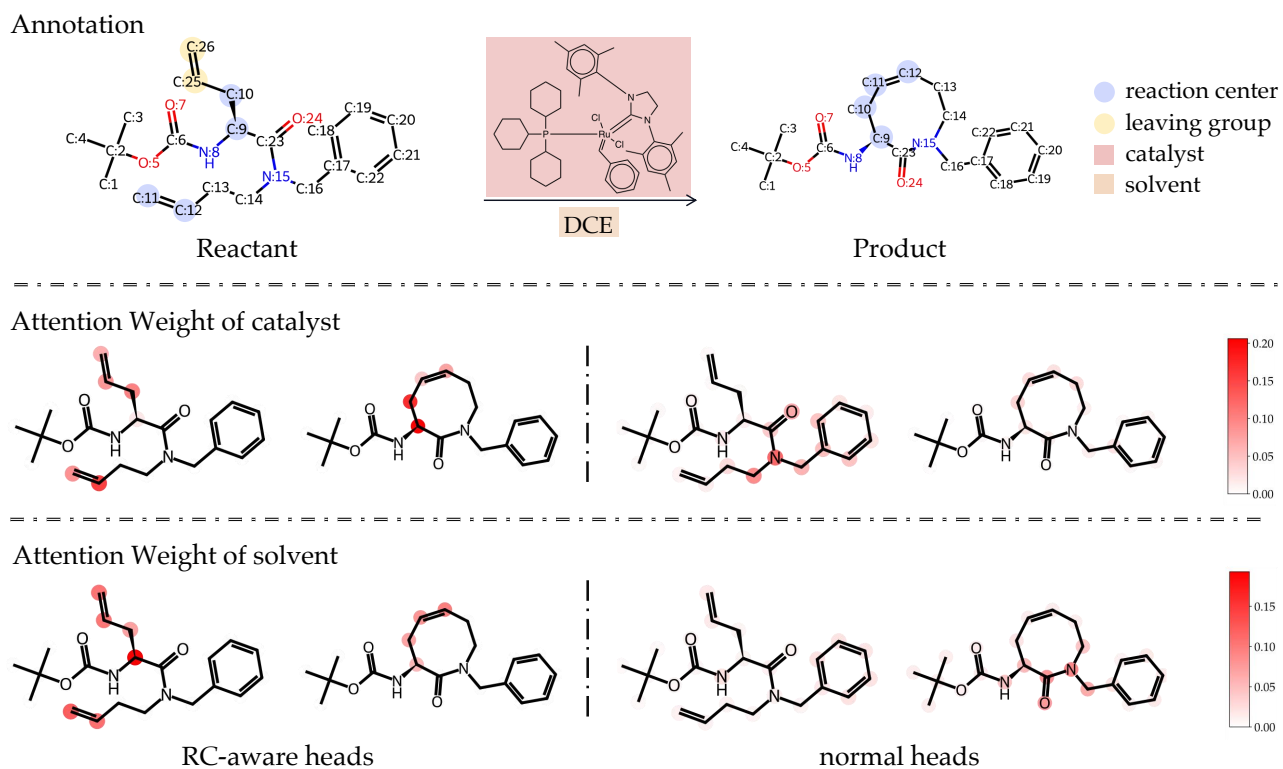


Figure 6. The visualization of the RC-aware cross attention coefficients for the reaction condition combination prediction of a olefin metathesis reaction.

more diverse, which is probably why our model is able to achieve better performance.

### A.3. Robustness of Our Model against Incorrect Atom-mapping

Existing atom-mapping tools are not entirely reliable, as there may be instances where these tools incorrectly match similar substructures between reactants and products. To investigate the robustness of our model against erroneous inputs from these atom-mapping tools, we explored the relationship between the accuracy of the model in predicting/generating chemical reaction conditions and the atom mapping confidence scores provided by RXNMapper (Schwaller et al., 2021a). We segmented the data from USPTO\_CONDITION and USPTO\_500MT based on the atom mapping confidence scores in increments of 0.1 and then calculated the top- $k$  accuracy within each interval. The results are depicted in Fig. 8. Additionally, we computed the Pearson correlation coefficients between the median confidence and the top- $k$  accuracy of samples within each interval, which are presented in Table 9.

Table 9. The Pearson correlation coefficient between the median confidence and the top- $k$  accuracy of samples within each interval

Dataset	top-1	top-3	top-5	top-10
USPTO_CONDITION	0.096	0.053	-0.020	-0.077
USPTO_500MT	-0.037	0.283	0.367	0.415

From the table and figure, we observe that there is no strong correlation between our model’s performance and the confidence of atom mapping. This indicates that although our model relies on atom mapping as input, it maintains a certain level of robustness against erroneous atom mapping, as long as the atom mapping can match similar substructures between reactants and products.

## B. Datasets

### B.1. Statistical Information of Datasets

We summarize the statistical information of all the datasets used in this work in Table 10.

Table 10. The statistical information of datasets in this work.

Dataset	Split-type	Train	Val	Test
USPTO_CONDITION	random split	544,591	68,075	68,075
USPTO_500MT	random split	116,360	12,937	14,238
Buchwald-Hartwig	random split	2,491	277	1187
	Test1	2,751	306	898
	Test2	2,749	306	900
	Test3	2,752	306	897
	Test4	2,749	306	900
thiol addition	random split	677	75	323
C-H functionalization	random split	3,851	428	1,835

### B.2. Metrics for evaluation

We use various metrics to evaluate task performance on different datasets. The USPTO\_CONDITION dataset serves as the benchmark for evaluating the Condition Prediction task, the USPTO\_500MT dataset is used for the Condition Generation task, the Buchwald-Hartwig dataset is employed for the Reaction Yield Prediction task, and the Thiol Addition and C-H Functionalization datasets are used for the Reaction Selectivity Prediction task.

- **Condition Prediction/Generation.** We assess the predictive performance for the whole reaction condition combinations as well as for each constituent element within the reaction conditions. We use the conventional top- $k$  accuracy to

- layer\_1\_reac   • layer\_4\_reac   • layer\_1\_prod   • layer\_4\_prod
- layer\_2\_reac   • layer\_5\_reac   • layer\_2\_prod   • layer\_5\_prod
- layer\_3\_reac   • layer\_6\_reac   • layer\_3\_prod   • layer\_6\_prod

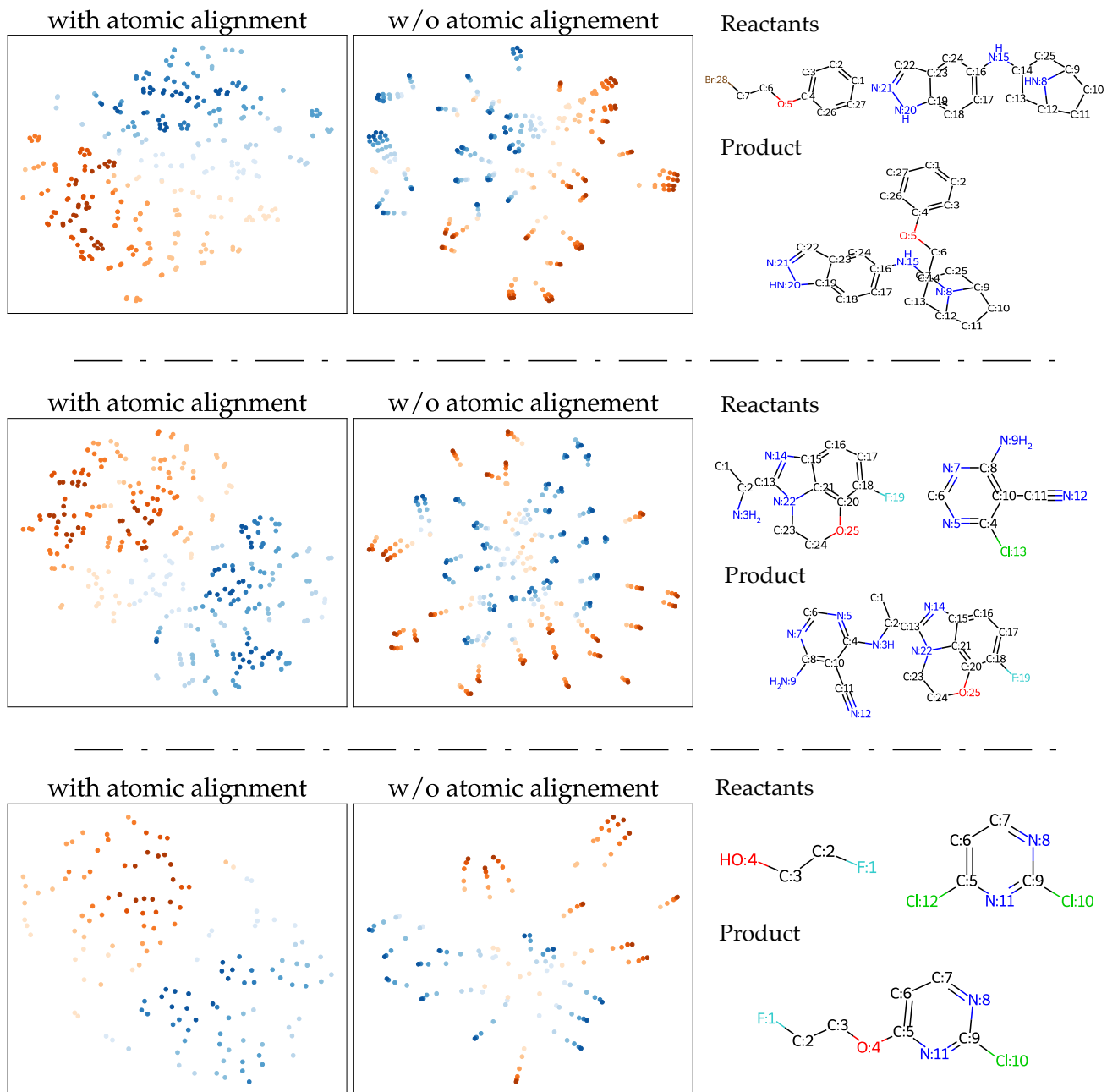


Figure 7. The visualizations of node embeddings at each encoder layer for different reactions, comparing the atom-aligned encoder with the conventional MPNN encoder.

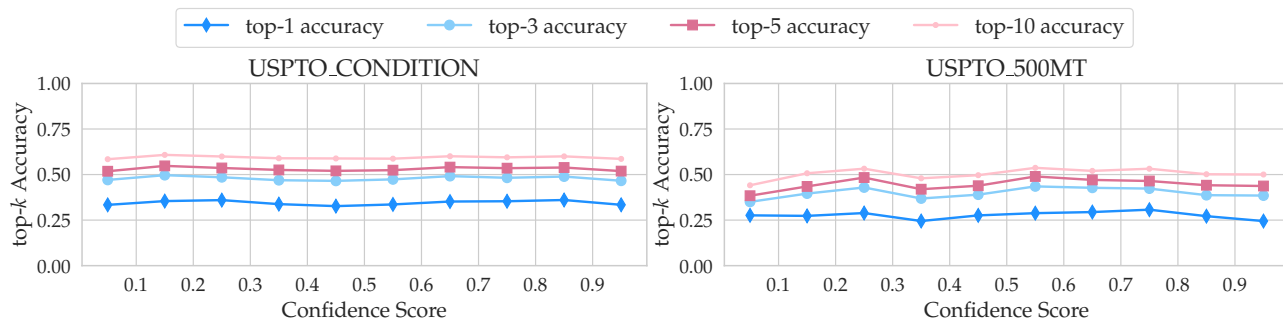


Figure 8. The relation between top- $k$  accuracy and the atom mapping confidence score on the USPTO\_CONDITION dataset and the USPTO\_500MT dataset.

evaluate the performance. A prediction is considered correct if and only if all of the molecules of it are correctly predicted. The order of the constituents is not one of the criteria for determining whether a prediction is correct. When a reaction in the test set has multiple recorded reaction combinations, a prediction is considered correct if it is completely consistent with any one of them.

- **Reaction Yield/Selectivity Prediction.** Datasets for these tasks provide the single numeric reaction output (yield or selectivity metric) as prediction targets, thus we could consider these tasks as regression problems, and use the conventional metrics including  $R^2$  score, root mean square error (RMSE), and mean absolute error (MAE), for evaluation.

## C. Implementation Details

### C.1. Pipeline for different tasks

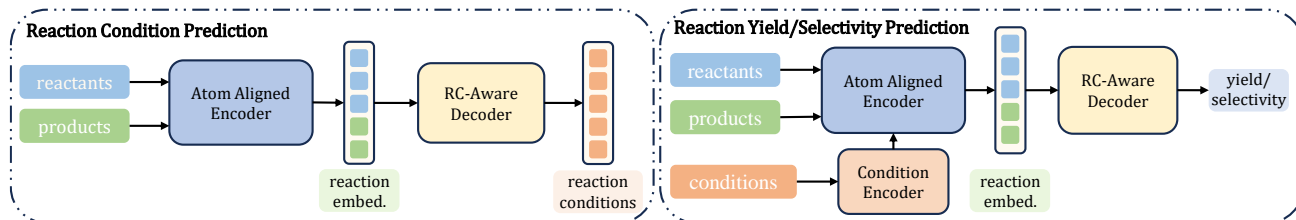


Figure 9. The pipelines for different tasks

This work does not train a multi-task unified model like T5chem (Lu & Zhang, 2022). Given the different datasets and varying inputs and outputs for each task, we have selected different modules to assemble the pipelines for the tasks discussed in this paper. The two pipelines involved are displayed in Fig. 9. The input for the reaction condition prediction task consists solely of reactants and products, hence the pipeline for this task is composed of an atom-aligned encoder followed by a RC-aware decoder with sequential output. For the reaction yield prediction and reaction selectivity prediction tasks, which also include reaction conditions in their input, we have incorporated a reaction condition encoder and utilized a RC-aware decoder with single output.

### C.2. Initial node/edge feature extraction

We use the atom and bond encoder provided by Open Graph Benchmark (Hu et al., 2020a). These encoders transform the atom and chemical bonds into integer numbers based on their characteristics and molecular structure. Nine atom descriptors are provided, including the atom type, formal charge, and other properties that can be calculated by RDKit (Landrum et al., 2013). As for chemical bonds, three descriptors are used, including bond type, bond stereochemistry, as well as whether the

bond is conjugated. Every descriptor corresponds to a learnable embedding table. The initial node and edge features are derived by aggregating the embeddings corresponding to each descriptor.

### C.3. MPNN Layer in Atom Aligned Encoder

In contrast to many graphs where edges convey limited information, the chemical bonds within molecules play a pivotal role in determining their properties. Consequently, we employ a variant of the Graph Attention Network (Veličković et al., 2018), akin to those utilized in the works of Yan et al. and Sacha et al., to integrate information from chemical bonds into the node features during the message-passing process. The MPNN layer we implement can be mathematically formulated as follows:

$$\begin{aligned}
 \tilde{e}_{u,v} &= \text{FFN}_e(e_{u,v}), \\
 \tilde{h}_u &= \text{FFN}_n(h_u), \\
 c_{u,v} &= \mathbf{a}^T [\tilde{h}_u \parallel \tilde{h}_v \parallel \tilde{e}_{u,v}], \\
 \alpha_{u,v} &= \frac{\exp(\text{LeakyReLU}(c_{u,v}))}{\sum_{v' \in \mathcal{N}(u) \cup \{u\}} \exp(\text{LeakyReLU}(c_{u,v'}))}, \\
 h'_u &= \sum_{v \in \mathcal{N}(u) \cup \{u\}} \alpha_{u,v} (\tilde{h}_u + \tilde{e}_{u,v}^{(k)}),
 \end{aligned} \tag{8}$$

where  $h_u$  represents the input node feature of node  $u$ ,  $e_{u,v}$  represents the input edge feature of edge  $(u, v)$  and  $h'_u$  represents the output node feature of  $u$  of the message passing layer.

### C.4. Condition Encoders for Buchwald–Hartwig and thiol addition Selectivity Dataset

The Buchwald–Hartwig and thiol addition selectivity dataset uses chemical reagents as reaction conditions. To generate condition features, we employ a graph neural network. It should be noted that the number of distinct reagents in these datasets is quite limited, with fewer than 50 different molecules available, which makes it challenging to train a reaction condition encoder from scratch. Therefore, we have opted to use a pretrained molecular representation model proposed by Hu et al.. This model is lightweight and has been pretrained using only the random atom masking task. The roll-out form of the  $k$ -th layer of this model is formulated as

$$\begin{aligned}
 X &= \sum_{u \in \mathcal{N}(v) \cup \{v\}} h_u^{(k-1)} + \sum_{e=(u,v)} \sum_{u \in \mathcal{N}(v) \cup \{v\}} h_e^{(k-1)}, \\
 h_v^{(k)} &= \text{ReLU} \left( \text{MLP}^{(k)}(X) \right),
 \end{aligned} \tag{9}$$

where  $h_u^{(k)}$  is the node feature of node  $u$  in  $k$ -th layer and  $h_e^{(k)}$  is the edge feature of edge  $e$  in  $k$ -th layer. Using this pretrained model does not compromise the fairness of our experiments, as our compared baselines are also pretrained on chemical reaction datasets. Moreover, this further illustrates that our design can efficiently integrate existing works for chemical reaction representation learning, even if these works were not specifically designed for chemical reactions.

### C.5. Model Implementation details

We implement our model based on `torch_geometric 2.2.0` (Fey & Lenssen, 2019) and `Pytorch 1.13` (Paszke et al., 2019). For the model for reaction condition prediction, we set the hidden size as 512, encoder layers as 6, decoder layers as 6, and the number of attention heads as 8. The dropout ratio is set as 0.1. The highest learning rate of each model is set as 1.25e-4. We slowly increase our learning rate to the highest in the first few epochs and slowly decrease it using exponential decay. For reaction yield prediction, we set the hidden size as 128, encoder layers as 3, and attention heads as 8. The dropout ratio is set as 0.1, and the learning rate is set as 1e-4. For reaction selectivity prediction in the Thiol addition dataset, we set the hidden size as 128, encoder layers as 3, and attention heads as 8. The dropout ratio is set as 0.0, and the learning rate is set as 5e-5. For reaction selectivity prediction on the C-H functionalization dataset, we set the hidden size as 128, encoder layers as 5, and attention heads as 8. The dropout ratio is set as 0.0 and the learning rate is set as 5e-4. All models are trained with the Adam optimizer (Kingma & Ba, 2014). We will consider open-sourcing our code upon the paper acceptance.

## D. Data Preparation

### D.1. Adding Atom-mapping

The Buchwald-Hartwig dataset features a consistent reaction template across all its reaction data, enabling the derivation of atom-mapping through rule-based approaches. For all the other datasets except the Buchwald-Hartwig dataset, we have employed Rxnmapper (Schwaller et al., 2021a) to obtain atom-mapping. It is noteworthy that we have re-annotated the labels for the USPTO\_500MT dataset, treating both the originally provided reactants and reagents as input reactants during the atom mapping annotation for this dataset. For further details on the processing of the USPTO\_500MT dataset, please refer to Appendix D.2.

### D.2. Generation of Reagents of USPTO\_500MT

We restructured our dataset. Following the annotations provided by the dataset, we divided the reactants involved in the reactions into a series of charge-balanced ions or molecular clusters. Here, we treat a cluster as a single molecule, rather than segmenting molecules based on the delimiter ‘.’ as in prior studies. Utilizing RXNMapper (Schwaller et al., 2021a), we appended atom-mapping to the reactions, where molecules in the original reactants that have atoms present in the products are considered reactants, and the remaining portions are classified as reagents. We categorized the reagents according to the following hierarchy:

- If a molecule is a free metal, or it contains a cyclic structure along with a metal or phosphorus atom, or it is a metal halide, it is designated as Type I.
- If a molecule is an organic compound, it is designated as Type II.
- The remaining molecules are categorized as Type III.

Our data labels are constructed in the order of Type I, Type II, and Type III. When reagents contain multiple molecules of the same type, these molecules are sorted in ascending order of their SMILES string lengths within the same category.

## E. Baselines

### E.1. Chemical Reaction Condition Prediction

We choose T5Chem (Lu & Zhang, 2022), Parrot-LM\_E (Wang et al., 2023), GCNN (Maser et al., 2021), Reagent Transformer (Andronov et al., 2023), and FPRCR (Gao et al., 2018) as our baselines for Chemical Reaction Condition Prediction; the details of them are as follows.

- Parrot-LM\_E is a transformer-based model. It takes the SMILES of the reaction as input to predict the chemical reaction condition combinations. It is specifically designed for reaction condition combinations with a fixed number of components and it is developed from the checkpoint of BERT (Devlin et al., 2019).
- Reagent Transformer is also a transformer-based model. It is developed from the checkpoint provided by Molecular Transformer (Schwaller et al., 2019), a model pretrained on predicting chemical reaction products. It should be noted that in the original design of Reagent Transformer, the decoder is used to generate SMILES strings. For a fair comparison, we replaced the original vocabulary optimized for SMILES generation with a predefined molecular library and adapted the reaction condition prediction problem into a sequence generation task with a fixed length of 5.
- T5Chem is a language model pretrained on the PubMed dataset (Kim et al., 2020) with a self-supervised task and the USPTO\_500MT dataset (Lu & Zhang, 2022) with five different supervised tasks including chemical reaction condition generation. Similar with Reagent Transformer, the decoder of T5Chem is designed for SMILES generation. Thus, we replaced the original vocabulary optimized for SMILES generation with a predefined molecular library and adapted the reaction condition prediction problem into a sequence generation task with a fixed length of 5.
- FPRCR is a fingerprint-based method specifically designed for reaction condition combinations with a fixed number of components. The model comprises a set of MLPs that correspond to the number of components in the reaction condition combination. All MLPs are invoked in the order of prediction, taking the fingerprints of reactants, products,

and the already predicted reaction condition combination components as input to forecast the next molecule that should be used as a condition.

- GCNN is a graph-based method that takes the molecular graphs of reactants and products as input to generate chemical reaction representations for predicting reaction condition combinations. The reaction condition combinations in the USPTO\_CONDITION dataset are composed of up to one catalyst, two solvents, and two reagents. We have extended the model’s prediction head from a single multilabel classification head to five separate single-label classification heads.

## E.2. Chemical Reaction Condition Generation

We choose GCNN (Maser et al., 2021), Reagent Transformer (Andronov et al., 2023), and T5Chem (Lu & Zhang, 2022) for Chemical Reaction Generation Prediction. The details of them are as follows.

- Reagent Transformer is a transformer-based model. It is developed from the checkpoint provided by Molecular Transformer (Schwaller et al., 2019), a model pretrained on predicting chemical reaction products. It’s originally designed for SMILES generation so we do not make any modification.
- T5Chem is a language model pretrained on the PubMed dataset (Kim et al., 2020) with a self-supervised task and the USPTO\_500MT dataset (Lu & Zhang, 2022) with five different supervised tasks including chemical reaction condition generation. In this paper, we present the results of two versions of T5Chem. One is developed from the pretrained checkpoint and the other is trained from scratch on only the chemical reaction condition generation task.
- GCNN is a graph-based method that takes the molecular graphs of reactants and products as input to generate chemical reaction representations for predicting reaction condition combinations. The original design of it is not suitable for SMILES generation, so we follow the original design of it and formulate the chemical reaction condition generation task on USPTO\_500MT as multilabel classification problem for it. The labels here is to present whether a molecule in the predefined molecular library could be a part of the reaction condition combination, and use the combinations with the  $k$ -highest probabilities to calculate top- $k$  accuracy.

## E.3. Chemical Reaction Yield/Selectivity Prediction

The tasks of predicting chemical reaction yield and selectivity are highly analogous regression tasks; hence, their baselines are identical. **It is noteworthy that the emphasis of this paper is on introducing a novel architecture for chemical reaction representation learning, rather than being limited to the specific task of Chemical Reaction Yield/Selectivity Prediction.** Therefore, we have not included baselines with complex pretraining tasks or intricate training loss and inference strategies. Pretraining and specialized loss functions tailored for Reaction Yield Prediction are orthogonal to our research. The details of the chosen baselines are as follows.

- DRFP (Probst et al., 2022) is a kind of chemical reaction fingerprint for yield prediction, which calculates the fingerprint of the symmetric difference between the n-grams of reactants and products.
- MFF (Sandfort et al., 2020) uses multiple fingerprint features of all molecules in one reaction as the input of the regressor.
- Chemprop (Heid et al., 2024) is a kind of Message Passing Network encoding reactions. It converts the reactant and product SMILES pairs into a single pseudo-molecule, known as the condensed graph representation (CGR) of the reaction, and processes it through a directed messaging passing network (D-MPNN) to extract reaction features.
- RXNFP (Schwaller et al., 2021b) is a transformer model that has been pre-trained on the Pistachio dataset (Mayfield et al., 2017) utilizing self-supervised learning tasks. Building upon this work, the original research team has also proposed a finetuned version for predicting chemical reaction yields, termed YieldBert (Schwaller et al., 2021c).
- T5Chem (Lu & Zhang, 2022) is a language model pretrained on the PubMed dataset (Kim et al., 2020) with a self-supervised task and the USPTO\_500MT dataset (Lu & Zhang, 2022) with five different supervised tasks including reaction yield prediction.